

Supporting Information

Surface Modulus Reconstruction toward Robust Flexible Perovskite Solar Cells

Zheng Lu ^{a,#}, Xiaoli Xu ^{c,#}, Yanhui Lou ^{b,*}, Lingbo Xiao ^b, Jie Zhao ^b, Shuai Zou ^a,

Yingzhuang Ma ^{a,d}, Lutao Li ^b, Chen Wang ^b, Xiaodong Su ^{a,*}, Guifu Zou ^{b,*}

^a School of Physical Science and Technology, Jiangsu Key Laboratory of Thin Films, Soochow University, Suzhou 215006, China.

^b Key Laboratory of Advanced Carbon Materials and Wearable Energy Technologies of Jiangsu Province, College of Energy, Soochow University, Suzhou 215006, China.

^c College of Materials and Chemistry, China Jiliang University, Hangzhou 310018, China.

^d School of Optical and Electronic Information, Suzhou City University, Suzhou, Jiangsu 215104, China

These authors contributed equally to this work.

* Corresponding authors

E-mail addresses: yhlou@suda.edu.cn (Y. Lou), xdsu@suda.edu.cn (X. Su), zougufu@suda.edu.cn (G. Zou).

Experimental section

Materials:

All the purchased materials were used as received without further purification. Cesium iodide (CsI) was purchased from Aladdin, PTAA, Lead iodide (PbI₂), Formamidinium iodide (FAI), Formamidinium bromide (FABr), Lead chloride (PbCl₂), PCBM, BCP were purchased from Xi'an Polymer Light Technology Corp. Dimethylsulfoxide (DMSO, 99.8%), chlorobenzene (CB, 99.8%) and N, N'-dimethylformamide (DMF, 99.8%) were purchased from Alfa, and TPEE was purchased from DuPont Company. PEN/ITO and glass/ITO substrates were purchased from Advanced Election Technology Co., Ltd.

Device Fabrication:

The PTAA (2 mg/mL in CB) solution was spin-coated onto the PEN/ITO substrate at a speed of 4000 rpm for 30 s. The perovskite precursor solution was prepared by dissolving 591.3 mg PbI₂, 185.7 mg FAI, 18.8 mg PbCl₂, 8.5 mg FABr, and 52.6 mg CsI in a mixed solvent of 800 μ l DMF and 200 μ l of DMSO, and it was stirred at 65 °C for 2 hours. After the solution was completely dissolved and filtered, 60 μ l of perovskite solution was spin-coated onto the PTAA film at a speed of 1000 rpm for 10 s and 4000 rpm for 25 s. In this process, CB as an anti-solvent was added dropwise within 30 s. After annealing at 110 °C for 1 min and natural cooling, different concentrations (1-10 mg/mL, the solvent is chlorobenzene) of TPEE (5000 rpm for 15 s) were spin-coated onto the perovskite film and annealed at 110 °C for 19

min. Then, the PCBM solution (20 mg/mL in CB) and BCP (0.5 mg/mL in ethanol) were spin-coated onto the TPEE film. At last, a 100 nm silver electrode was deposited by thermal evaporation. The effective area of the PSCs is 0.0725 cm². The preparation process of the test samples is the same as that of the device preparation before evaporation.

Calculation formula:

The bending test: For the multilayer films, the relationship between film stress and curvature radius is shown as follows: $\sigma_f = \frac{E_f h_f^2}{6(1 - \nu_s)R}$, σ_f is the value of stress, E_f is Young's modulus of film, h_f is the thickness of the film, ν_s is the Poisson's ratio of film and R is curvature radius.

Trap density calculation: The formula for calculating the trap density is $N_{\text{trap}} = 2\varepsilon_r \varepsilon_0 V_{TFL} / qL^2$, where V_{TFL} refers to the starting voltage of the trap filling limit, q is the basic charge of the electron ($q = 1.6 \times 10^{-19}$ C), L is the thickness of perovskite layer, ε_0 is the vacuum permittivity ($\varepsilon_0 = 8.854 \times 10^{-12}$ F/m), and ε_r is the relative dielectric constant.

V_{oc} and J_{sc} as a function of incident light intensity (I) are fitted via the following equations: $J_{sc} \propto I^\alpha$, and $V_{oc} = nkT \ln(I)/q + \text{constant}$, respectively. k represents the Boltzmann constant, q is the elementary charge, T is absolute temperature, and α and n represent factors related to bimolecular and monomolecular recombination, respectively.

Measurement and Characterization:

The scanning electron microscope images were measured by a scanning electron microscope (Hitachi SU8010). The current density-voltage curves were obtained by a programmable Keithley 2400 source meter at $100 \text{ mW}\cdot\text{cm}^{-2}$ under AM 1.5 G solar irradiation (SAN-EI, AAA Class Solar Simulator, XES-70S1). The X-ray diffraction patterns were measured by an X-ray diffractometer (Bruker D8 Advance). The optical transmission spectrum was measured by Lambda 750S. The incident photo-to-current efficiency curve was performed by QE-R3018. The Pb 4f and I 3d were characterized by X-ray photoelectron spectroscopy (Thermo Fisher, Escalab 250Xi). The topography and modulus of the films were obtained by atomic force microscopy (Bruker Dimension Icon). The probe Tap300A (Nanoworld Co., Ltd, thickness: $4 \text{ }\mu\text{m}$, length: $125 \text{ }\mu\text{m}$, width: $30 \text{ }\mu\text{m}$, resonance frequency: 300 kHz) was used for mechanical AFM test, with a nominal spring constant $k = 40 \text{ N/m}$, and it is suitable for a studied modulus range from 0.2 GPa up to tens of GPa . The deflection sensitivity was measured with a sapphire surface. The scanning size was $2 \times 2 \text{ }\mu\text{m}^2$ for all the measurements. The maximum force in PeakForce Quantitative Nanomechanical Mapping mode ranged from 50 to 250 nN . The steady-state and time-resolved PL spectra were measured by FLS 1000 (Edinburgh Instruments Co., Ltd). The bending tests of the f-PSCs used a set of an assembled electric linear sliding table (Zolix Instruments Co., Ltd). Stress-strain tests used a high-performance motorized test stand (ESM303).

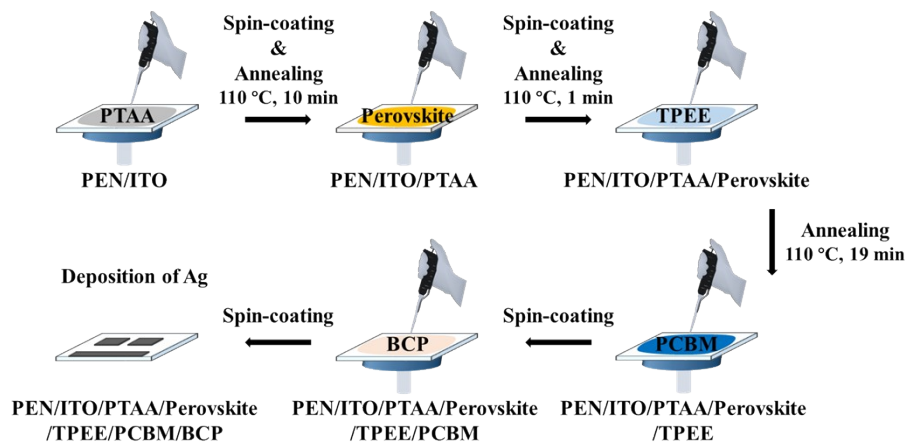


Fig. S1. Schematic diagram of the device fabrication process.

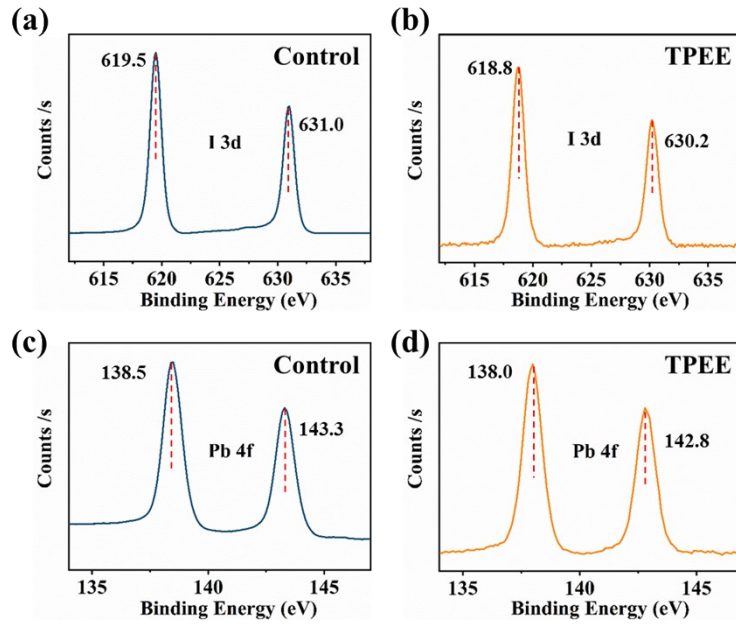


Fig. S2. X-ray photoelectron spectroscopy spectra of I element in the (a) control and (b) TPEE-coated perovskite film and Pb element in the (c) control and (d) TPEE-coated perovskite film.

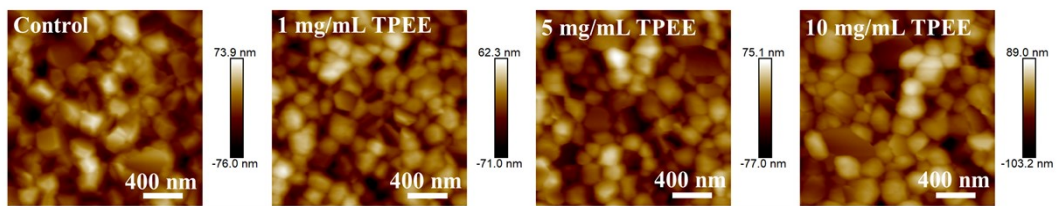


Fig. S3. Height AFM images of (a) control perovskite film, (b-d) different concentrations of TPEE coated on perovskite films.

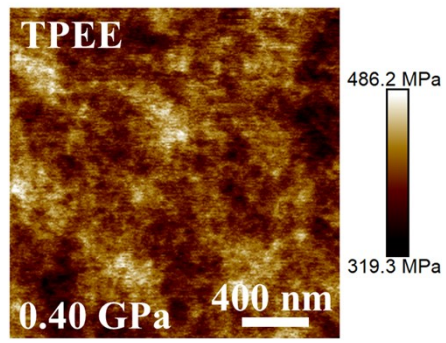


Fig. S4. Mechanical AFM image of TPEE film.

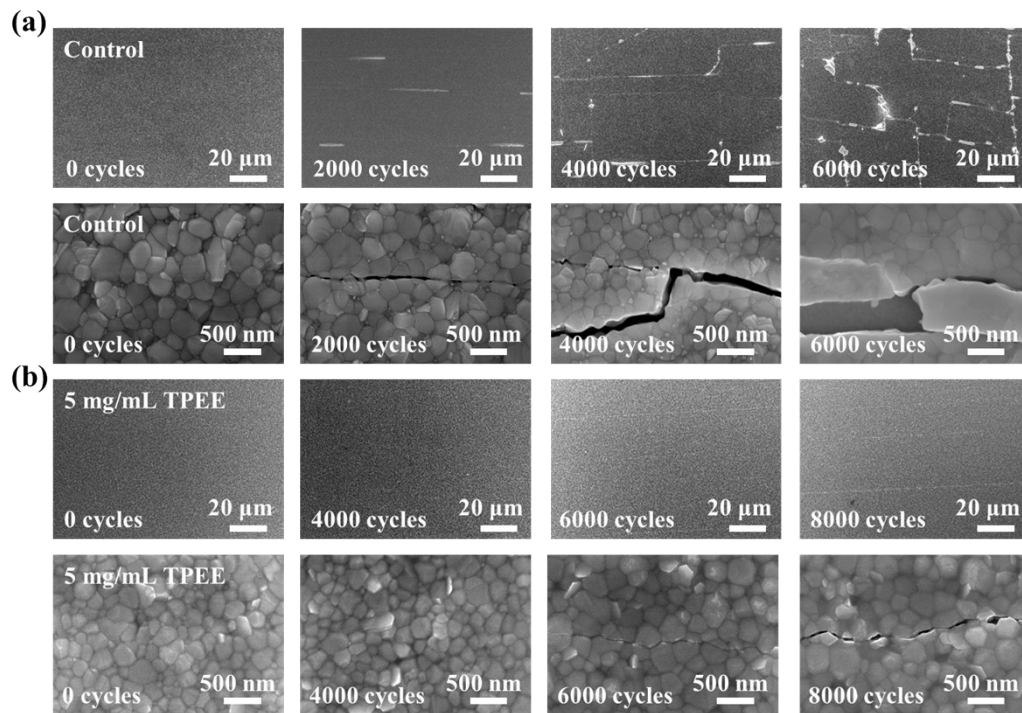


Fig. S5. SEM images of (a) the control perovskite film and (b) TPEE-coated perovskite film bend for different cycles at a 2 mm curvature radius.

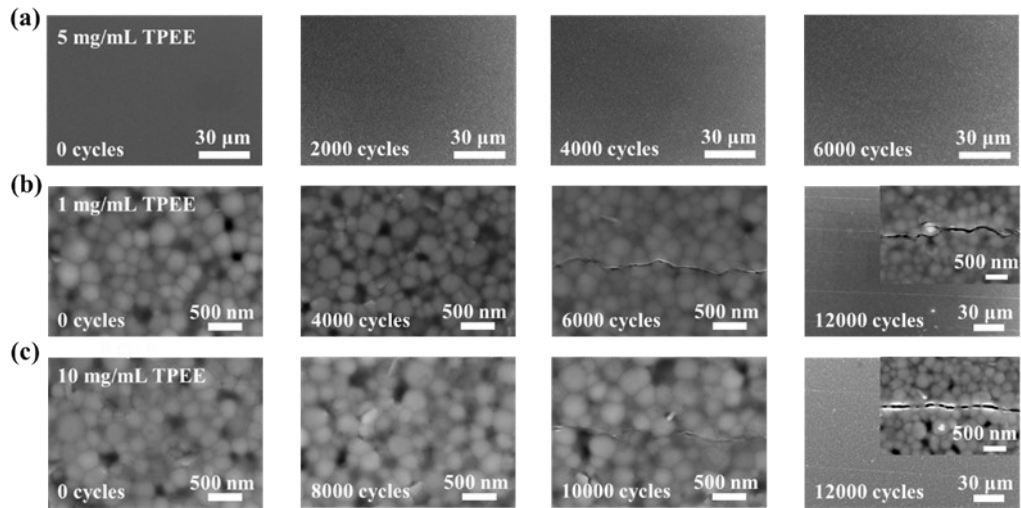


Fig. S6. SEM images of the perovskite/TPEE/PCBM film bent for different cycles at a 2 mm curvature radius. The concentration of TPEE is (a) 5 mg/mL, (b) 1 mg/mL, and (c) 10 mg/mL.



Fig. S7. The geometric model for bending simulation in finite element analysis. The design of this two-dimensional model is proportional, and the size of the geometric unit is 250 nm, which can match the grain size of perovskite films.

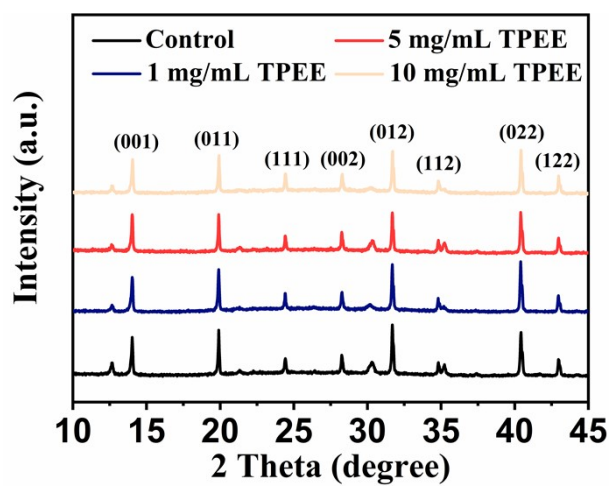


Fig. S8. X-ray diffraction patterns of the control and TPEE-coated perovskite films.

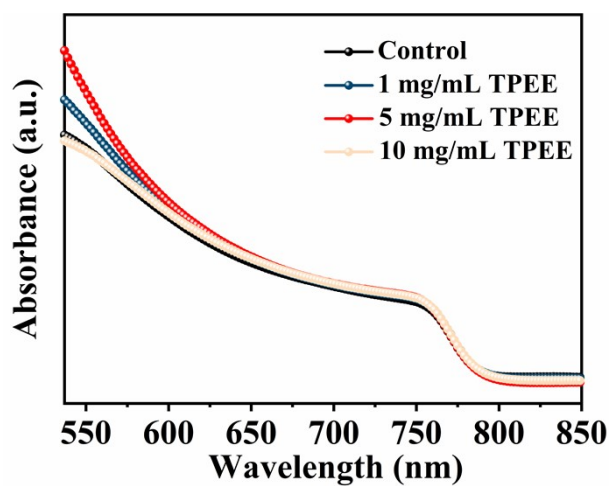


Fig. S9. Absorption spectra of the control and TPEE-coated perovskite films.

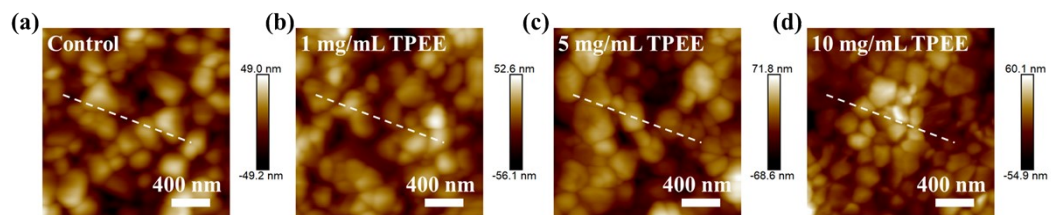


Fig. S10. Height AFM images of (a) control perovskite film, (b-d) different concentrations of TPEE coated on perovskite films.

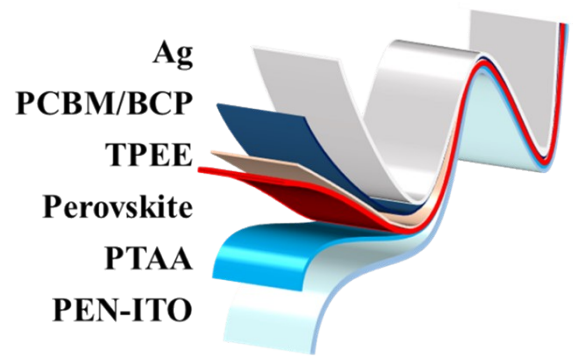


Fig. S11. Schematic diagram of the f-PSCs structure (PEN/ITO/poly(triarylamine) (PTAA)/perovskite/TPEE/PCBM)/bathocuproine (BCP)/Ag).

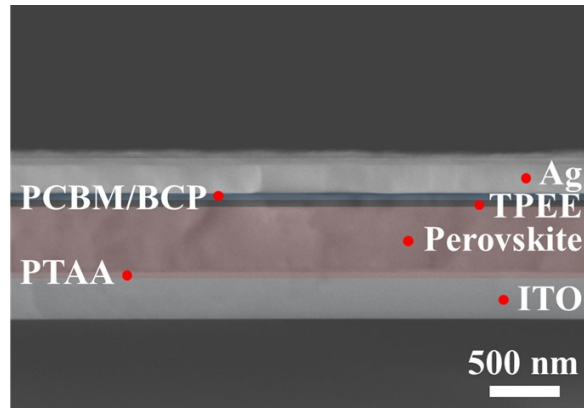


Fig. S12. SEM cross-section images of the TPEE-based f-PSCs.

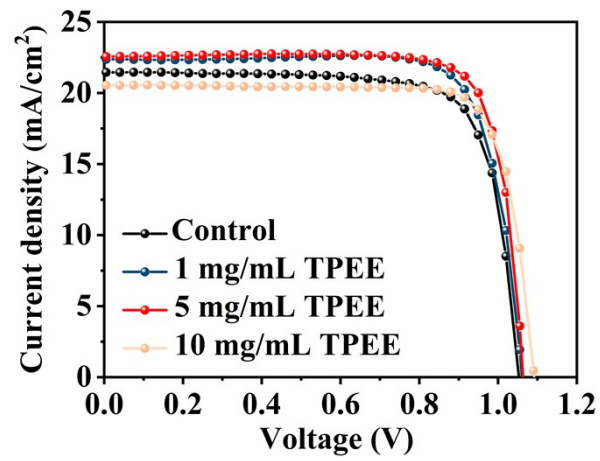


Fig. S13. J - V curves of the champion PCE of the f-PSCs based on different concentrations of TPEE.

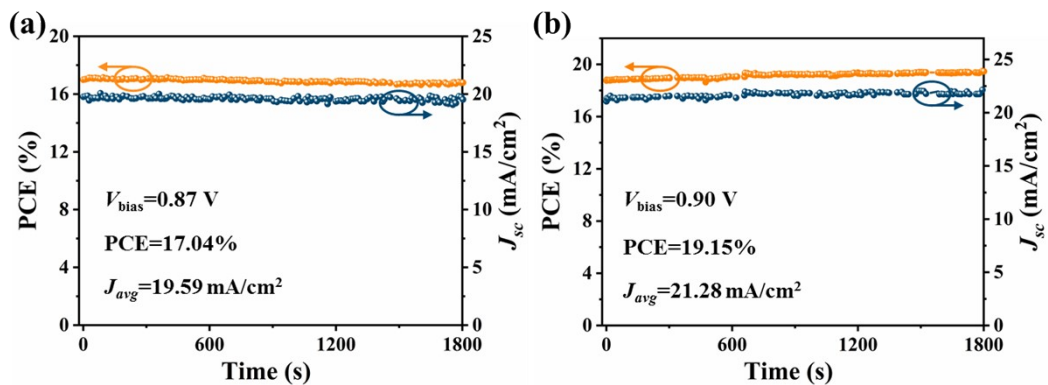


Fig. S14. (a) Steady-state average photocurrent and average output PCE of the control f-PSCs were measured under a constant bias voltage (0.87 V) near the maximum power point for 1800 s. (b) Steady-state average photocurrent and average output PCE of the TPEE-based f-PSCs were measured under a constant bias voltage (0.90 V) near the maximum power point for 1800 s.

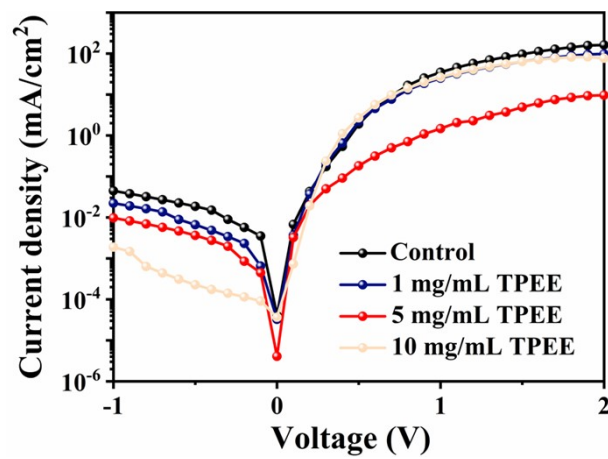


Fig. S15. Dark J - V curves of the devices based on different concentrations of TPEE.

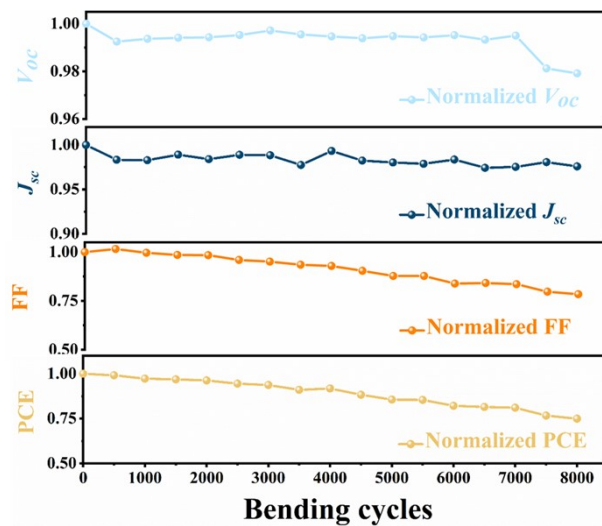


Fig. S16. The main photovoltaic parameters of the control f-PSCs with different bending cycles at a 2 mm curvature radius.

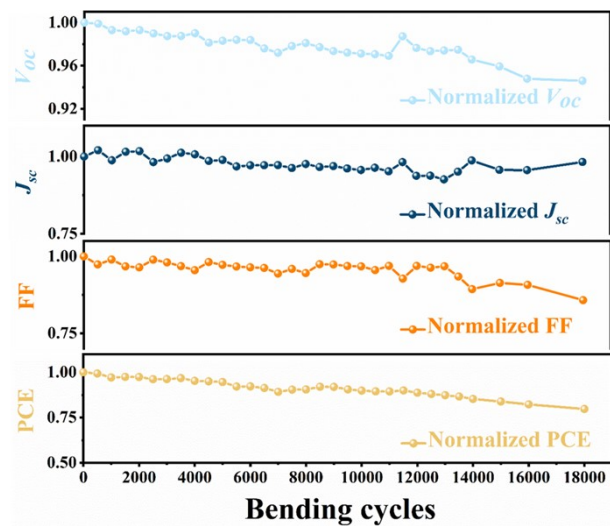


Fig. S17. The main photovoltaic parameters of the TPEE-based f-PSCs with different bending cycles at a 2 mm curvature radius.

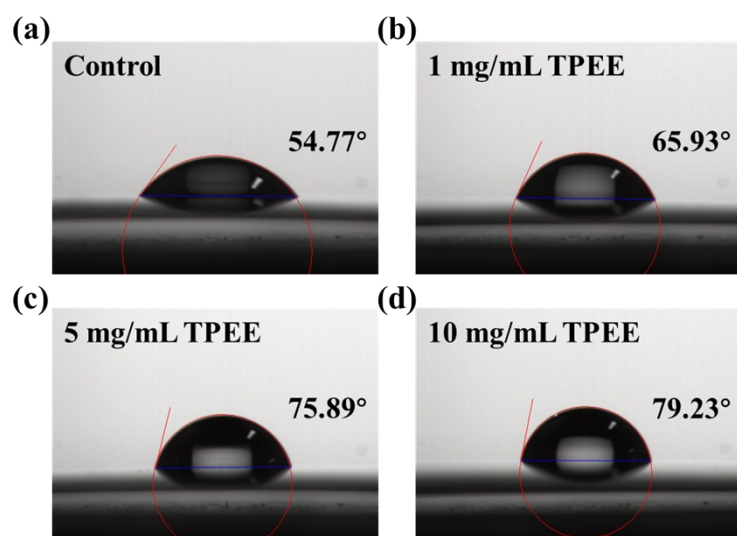


Fig. S18. (a-d) Water contact angles of perovskite films coated with different concentrations of TPEE.

Table S1. Physical parameters of different materials for finite element simulation.

Material	Thickness (nm)	Young's Modulus (GPa)	Density (ρ , g/cm ³)	Poisson's ratio
Perovskite	500	5.23	4.15	0.33
TPEE	10	0.40	1.15	0.42
PCBM	60	3.78	1.60	0.36

Table S2. The full width at half maxima (FWHM) of the (001) crystal orientation for the control and TPEE-coated perovskite films.

Sample	FWHM (°)
Control	0.151
1 mg/mL TPEE	0.143
5 mg/mL TPEE	0.136
10 mg/mL TPEE	0.142

Table S3. Trap density of control device and devices based on different concentrations of TPEE.

Sample	$N_{trap} (\text{cm}^{-3})$
Control	6.81×10^{15}
1 mg/mL TPEE	5.63×10^{15}
5 mg/mL TPEE	3.93×10^{15}
10 mg/mL TPEE	5.89×10^{15}

Table S4. Detailed photovoltaic parameters of control f-PSCs and TPEE-based f-PSCs.

Sample	V_{oc} (V)	J_{sc} (mA/cm ²)	FF (%)	PCE (%)
Control	1.05	21.45	76.87	17.36
1 mg/mL TPEE	1.06	22.37	78.67	18.71
5 mg/mL TPEE	1.07	22.55	80.44	19.38
10 mg/mL TPEE	1.09	20.54	80.33	18.02

Table S5. Photovoltaic parameters for different cycles of control f-PSCs bending at a 2 mm curvature radius.









Bending cycles	V_{oc} (V)	J_{sc} (mA/cm ²)	FF (%)	PCE (%)
0	1.0698	19.7918	78.9340	16.7134
500	1.0618	19.4623	80.1920	16.5722
1000	1.0630	19.4515	78.6203	16.2564
1500	1.0634	19.5758	77.7649	16.1897
2000	1.0637	19.4756	77.6715	16.0915
2500	1.0647	19.5716	75.7500	15.7851
3000	1.0667	19.5628	75.0516	15.6623
3500	1.0649	19.3462	73.8107	15.2076
4000	1.0641	19.6560	73.3477	15.3417
4500	1.0632	19.4423	71.3361	14.7471
5000	1.0642	19.4006	69.2907	14.3069
5500	1.0636	19.3717	69.2621	14.2715
6000	1.0646	19.4673	66.2112	13.7231
6500	1.0626	19.2833	66.4289	13.6127
7000	1.0644	19.3027	65.9637	13.5539
7500	1.0497	19.4097	62.9005	12.8166
8000	1.0475	19.3139	61.9065	12.5246

Table S6. Photovoltaic parameters for different cycles of TPEE-based f-PSCs bending at a 2 mm curvature radius.

Bending cycles	V_{oc} (V)	J_{sc} (mA/cm ²)	FF (%)	PCE (%)
0	1.0772	21.4292	77.7166	17.9409
500	1.0761	21.8758	75.6938	17.8191
1000	1.0697	21.1712	76.9226	17.4207
1500	1.0685	21.7635	75.2019	17.4886
2000	1.0697	21.8019	74.9418	17.4778
2500	1.0663	21.0497	76.8739	17.2552
3000	1.0637	21.2998	76.2032	17.2652
3500	1.0639	21.6980	75.2540	17.3721
4000	1.0665	21.5891	74.2429	17.0957
4500	1.0571	21.1312	76.2815	17.0409
5000	1.0590	21.2007	75.6020	16.9752
5500	1.0600	20.7485	75.1629	16.5322
6000	1.0598	20.8242	74.9639	16.5447
6500	1.0514	20.8274	74.8149	16.3830
7000	1.0471	20.8371	73.3703	16.0084
7500	1.0537	20.6421	74.5691	16.2201
8000	1.0568	20.9107	73.5141	16.2457
8500	1.0527	20.7034	75.7536	16.5107
9000	1.0487	20.7727	75.6921	16.4900
9500	1.0472	20.6024	75.2941	16.2453
10000	1.0463	20.4945	75.2053	16.1269
10500	1.0456	20.6595	74.2727	16.0454
11000	1.0439	20.4028	75.3058	16.0395
11500	1.0635	21.0490	72.0989	16.1404
12000	1.0519	20.0959	75.3233	15.9231
12500	1.0486	20.1074	74.8721	15.7872
13000	1.0493	19.8461	75.2178	15.6641
13500	1.0500	20.3769	72.6234	15.5396
14000	1.0403	21.1665	69.4617	15.2965
15000	1.0334	20.5094	71.0110	15.0515
16000	1.0211	20.4923	70.5347	14.7598
18000	1.0190	21.0515	66.6865	14.3066

Table S7. The summary of normalized PCE and different bending conditions of recently reported f-PSCs. The colorful circles represent different references corresponding to Fig. 5i.

Device structure	PCE (%)	Mechanical durability	Normalized PCE	Reference
PEN/ITO/PTAA/Perovskite/ TPEE/PC ₆₁ BM/BCP/Ag	19.38	Bending at 2 mm radius for 10000 cycles	0.90	★ This work
PEN/ITO/PTAA/Perovskite/ TPEE/PC ₆₁ BM/BCP/Ag	19.38	Bending at 2 mm radius for 18000 cycles	0.80	★ This work
PET/ITO/NiO _x /PMMA /perovskite/PC ₆₁ BM /BCP/Ag	20.01	Bending at 5 mm radius for 1000 cycles	0.90	● [1]
PEN/ITO/PEDOT:PSS /PTAA/Perovskite /PC ₆₁ BM/BCP/Ag	19.41	Bending at 3 mm radius for 1000 cycles	0.84	● [2]
PET/ITO/RT-SnO ₂ /Perovskite /Spiro-OMeTAD/Au	19.30	Bending at 5 mm radius for 10000 cycles	0.91	● [3]
PET/Ni mesh-PH1000 /PEDOT:PSS-NiO _x /Perovskite/PC ₆₁ BM/BCP/A g	17.30	Bending at 4 mm radius for 2000 cycles	0.76	● [4]
PEN/ITO/SnO ₂ /Y6 /Perovskite/SpiroOMeTAD/ MoO ₃ /Au	20.09	Bending at 8 mm radius for 1000 cycles	0.80	● [5]

PET/ITO/PEDOT:EVA /Perovskite/PC ₆₁ BM /BCP/Ag	19.87	Bending at 3 mm radius for 7000 cycles	0.85		[6]
PEN/ITO/FI-SnO ₂ /Perovskite /Spiro-OMeTAD/Au	20.10	Bending at 3 mm radius for 2500 cycles	0.85		[7]
PET/ITO/SnO ₂ /Perovskite/ Spiro-OMeTAD/Au	21.00	Bending at 5 mm radius for 10000 cycles	0.90		[8]
PEN/ITO/Bio-IL /Perovskite /PC ₆₁ BM/BCP/Ag	21.08	Bending at 3 mm radius for 2000 cycles	0.84		[9]
PEN/ITO/NiO _x /Perovskite/S piro-OMeTAD/Au	18.50	Bending at 7 mm radius for 1200 cycles	0.80		[10]
PEN/ITO/SnO ₂ -TiO ₂ /Perovskite/Spiro- OMeTAD/Au	21.02	Bending at 5 mm radius for 500 cycles	0.90		[11]
PEN/ITO/NiO _x :PDA /Perovskite /PC ₆₁ BM/BCP/Ag	16.23	Bending at 8 mm radius for 5000 cycles	0.72		[12]
PET/ITO/PEDOT:GO /Perovskite /PC ₆₁ BM/Ag	19.70	Bending at 3 mm radius for 5000 cycles	0.85		[13]

- [1] P. Ru, E. Bi, Y. Zhang, Y. Wang, W. Kong, Y. Sha, W. Tang, P. Zhang, Y. Wu, W. Chen, X. Yang, H. Chen, L. Han, High Electron Affinity Enables Fast Hole Extraction for Efficient Flexible Inverted Perovskite Solar Cells. *Adv. Energy Mater.* 10 (2020) 1903487.
- [2] Z. Wang, L. Zeng, C. Zhang, Y. Lu, S. Qiu, C. Wang, C. Liu, L. Pan, S. Wu, J. Hu, G. Liang, P. Fan, H. J. Egelhaaf, C. J. Brabec, F. Guo, Y. Mai, Rational Interface Design and Morphology Control for Blade-Coating Efficient Flexible Perovskite Solar Cells with a Record Fill Factor of 81%. *Adv. Funct. Mater.* 30 (2020) 2001240.
- [3] J. X. Zhong, W. Q. Wu, Y. Zhou, Q. Dong, P. Wang, H. Ma, Z. Wang, C. Y. Yao, X. Chen, G. I. Liu, Y. Shi, D. B. Kuang, Room Temperature Fabrication of SnO₂ Electrodes Enabling Barrier-Free Electron Extraction for Efficient Flexible Perovskite Photovoltaics. *Adv. Funct. Mater.* 32 (2022) 2200817.
- [4] M. Li, W. W. Zuo, A. G. Ricciardulli, Y. G. Yang, Y. H. Liu, Q. Wang, K. L. Wang, G. X. Li, M. Saliba, D. Di Girolamo, A. Abate, Z. K. Wang, Embedded Nickel-Mesh Transparent Electrodes for Highly Efficient and Mechanically Stable Flexible Perovskite Photovoltaics: Toward a Portable Mobile Energy Source. *Adv. Mater.* 32 (2020) 2003422.
- [5] H. Liu, Z. Zhang, Z. Su, W. Zuo, Y. Tang, F. Yang, X. Zhang, C. Qin, J. Yang, Z. Li, M. Li, Semi-Planar Non-Fullerene Molecules Enhance the Durability of Flexible Perovskite Solar Cells. *Adv. Sci.* 9 (2022) 2105739.
- [6] X. Meng, Z. Cai, Y. Zhang, X. Hu, Z. Xing, Z. Huang, Z. Huang, Y. Cui, T. Hu, M. Su, X. Liao, L. Zhang, F. Wang, Y. Song, Y. Chen, Bio-inspired vertebral design for scalable and flexible perovskite solar cells. *Nat. Commun.* 11 (2020) 3016.
- [7] Q. Dong, C. Zhu, M. Chen, C. Jiang, J. Guo, Y. Feng, Z. Dai, S. K. Yadavalli, M. Hu, X. Cao, Y. Li, Y. Huang, Z. Liu, Y. Shi, L. Wang, N. P. Padture, Y. Zhou, Interpenetrating interfaces for efficient perovskite solar cells with high operational stability and mechanical robustness. *Nat. Commun.* 12 (2021) 973.
- [8] Q. Dong, M. Chen, Y. Liu, F. T. Eickemeyer, W. Zhao, Z. Dai, Y. Yin, C. Jiang, J. Feng, S. Jin, S. Liu, S. M. Zakeeruddin, M. Grätzel, N. P. Padture, Y. Shi, Flexible perovskite solar cells with simultaneously improved efficiency, operational stability, and mechanical reliability. *Joule* 5 (2021) 1587-1601.
- [9] B. Fan, J. Xiong, Y. Zhang, C. Gong, F. Li, X. Meng, X. Hu, Z. Yuan, F. Wang, Y. Chen, A Bionic Interface to Suppress the Coffee-Ring Effect for Reliable and Flexible Perovskite Modules with a Near-90% Yield Rate. *Adv. Mater.* 34 (2022) 2201840.
- [10] W. Deng, F. Li, J. Li, M. Wang, Y. Hu, M. Liu, Anti-solvent free fabrication of FA-Based perovskite at low temperature towards to high performance flexible perovskite solar cells. *Nano Energy* 70 (2020) 104505.
- [11] M. J. Paik, J. W. Yoo, J. Park, E. Noh, H. Kim, S.-G. Ji, Y. Y. Kim, S. I. Seok, SnO₂-TiO₂ Hybrid Electron Transport Layer for Efficient and Flexible Perovskite Solar Cells. *ACS Energy Lett.* 7 (2022) 1864-1870.
- [12] X. Duan, X. Li, L. Tan, Z. Huang, J. Yang, G. Liu, Z. Lin, Y. Chen, Controlling

Crystal Growth via an Autonomously Longitudinal Scaffold for Planar Perovskite Solar Cells. *Adv. Mater.* 32 (2020) 2000617.

- [13] T. Xue, G. Chen, X. Hu, M. Su, Z. Huang, X. Meng, Z. Jin, J. Ma, Y. Zhang, Y. Song, Mechanically Robust and Flexible Perovskite Solar Cells via a Printable and Gelatinous Interface. *ACS Appl. Mater. Inter.* 13 (2021) 19959-19969.